

Widely-tunable optical parametric oscillator in lithium niobate nanophotonics

Luis Ledezma,^{1,2} Arkadev Roy,¹ Luis Costa,¹ Ryoto Sekine,¹ Robert Gray,¹
Qiushi Guo,¹ Rajveer Nehra,¹ Ryan M. Briggs,² and Alireza Marandi^{1,*}

¹*Department of Electrical Engineering, California Institute of Technology, Pasadena, California 91125, USA.*

²*Jet Propulsion Laboratory, California Institute of Technology, Pasadena, California 91109, USA.*

Widely-tunable coherent sources in nanophotonics are desirable for a multitude of applications ranging from communications to sensing. The mid-infrared spectral region (wavelengths beyond 2 μm) is particularly important for applications relying on molecular spectroscopy. Among tunable sources, optical parametric oscillators typically offer some of the broadest tuning ranges; however, their implementations in nanophotonics have been limited to modest tuning ranges and only at visible and near-infrared wavelengths. Here, we surpass these limits by demonstrating octave-spanning tunable optical parametric oscillators in dispersion-engineered periodically-poled lithium niobate nanophotonics. With a pump wavelength near 1 μm , we generate output wavelengths tunable from 1.53 μm to 3.25 μm , including common telecommunication bands and into the mid-infrared. Our results enable opportunities for numerous integrated photonic applications requiring compact tunable sources.

Widely-tunable coherent sources are vital for applications ranging from multi-channel optical communications [1] to lidar [2]. Wide tunability in the mid-infrared spectral range is especially desirable due to the rich molecular response of trace gases at wavelengths longer than 2 μm [3]. While it is possible to directly generate light at these wavelengths, e.g., using quantum cascade lasers, the tuning ranges available are typically narrow [4]. Alternatively, nonlinear optics provides flexibility on wavelength and tuning ranges, with optical parametric oscillators (OPO) being a prominent example that has commonly been realized using nonlinear crystals in bulky table-top setups not amenable to large-scale integration [5]. Thus, adopting OPOs as tunable sources in scalable optical systems requires developing compact OPOs. Previous efforts towards OPO miniaturization include using lithium niobate diffused waveguides with fiber feedback loops [6], semiconductor waveguides with Bragg mirrors deposited on the chip end-facets [7], and magnesium fluoride whispering-gallery microdisk resonators [8]. However, taking full advantage of OPOs as compact and widely tunable sources requires their implementation in nanophotonics, i.e., with waveguides providing sub-wavelength modal confinement and low propagation losses, which enable dispersion engineering through the waveguide geometry, small bending radii for dense integration with other on-chip components, and strong nonlinear interactions [9].

Over the past decade, progress in nanophotonic platforms development have led to OPO demonstrations in the near-infrared and visible ranges using materials with cubic ($\chi^{(3)}$) and quadratic ($\chi^{(2)}$) nonlinearities [10–13]. Despite these advances, implementation of widely-tunable OPOs in nanophotonics with mid-infrared coverage has been lacking so far. A noteworthy roadblock is the typical use of a triply-resonant configuration in

which all the interacting optical fields resonate simultaneously in a single microring. This leads to ultra-low OPO thresholds at the expense of an over-constrained system with complex and limited wavelength tunability. Instead of using triply-resonant configurations, operating OPOs in singly- or doubly-resonant configurations generally offers advantages with respect to tunability and frequency stability [5].

Here, we evidence these advantages by designing and demonstrating on-chip doubly-resonant OPOs with wavelengths tunable from 1.53 μm to 3.25 μm when pumped in the near infrared. We use the thin-film lithium niobate-on-silica platform and validate operation at wavelengths longer than previously predicted feasible [14]. These results establish an important milestone towards realizing widely tunable sources in nanophotonics.

To attain doubly-resonance, we design the OPO ring resonator using wavelength-selective couplers that allow the signal and idler wavelengths to resonate with a ~ 10 -GHz free spectral range, while letting the pump go only through the poled waveguide section [15]. Figure 1a shows a schematic of our design concept and Fig. 1b displays a false-color optical microscope image of one of our devices. Figure 1c, shows a simulated OPO gain surface, which describes the OPO tuning behavior. For instance, the three different pump wavelengths indicated by vertical lines in Fig. 1c produce the different parametric gain curves shown in Fig. 1d. The gain surface from Fig. 1c is obtained from conservation of energy ($\omega_p = \omega_s + \omega_i$) and momentum ($k_p = k_s + k_i + 2\pi/\Lambda_{QPM}$); thus it can be tailored by engineering the waveguide dispersion [16]. In particular, the tuning slope ($\partial\omega_s/\partial\omega_p$) is given by the ratio of group velocity differences $(1/v_i - 1/v_p)/(1/v_i - 1/v_s)$, while the gain-bandwidth is inversely proportional to $1/v_i - 1/v_s$.

When designing a tunable OPO, it is desirable to have a large tuning slope so a small change in pump wavelength produces large changes in the output wavelengths. At the same time, a small gain-bandwidth is preferable to limit the number of resonator modes experiencing gain.

* marandi@caltech.edu

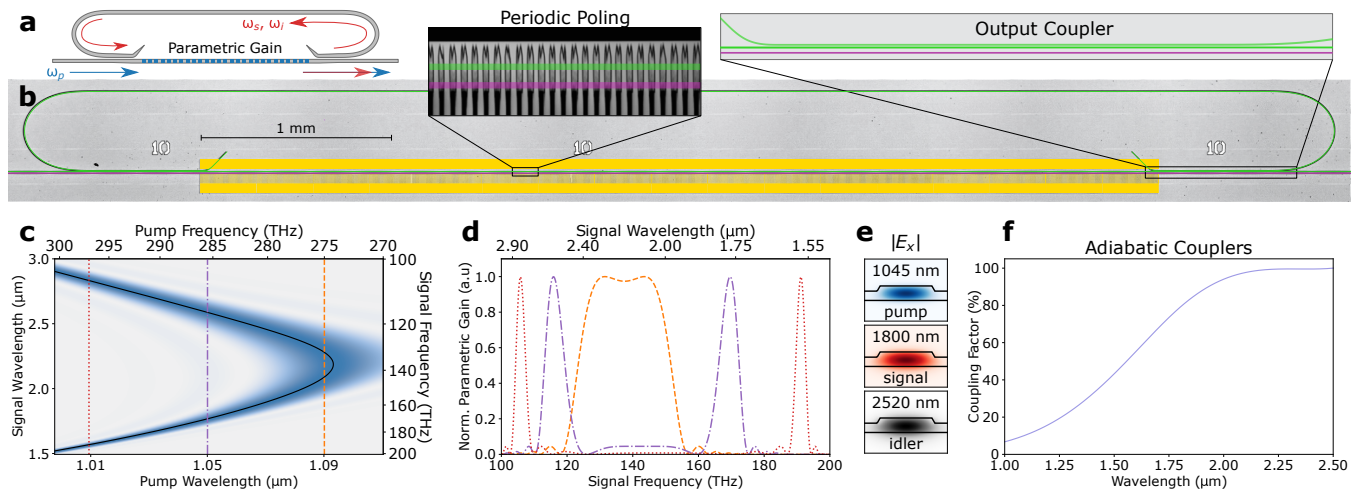


FIG. 1. **Doubly-resonant optical parametric oscillators in nanophotonics.** **a, b**, Schematic and false-color optical microscope image of a doubly-resonant OPO (green) and a straight waveguide (purple; used for calibration and phase-matching verification). Insets show a two-photon microscope image of the periodic poling and a close-up of the adiabatic output coupler. **c, d**, Simulated parametric gain surface (**c**) and curves (**d**). The black line in **c**, representing perfect phase matching, is the OPO tuning curve. The set of curves in **d** correspond to the vertical lines in **c**. **e**, Simulated mode profiles for a representative set of pump, signal, and idler wavelengths. **f**, Simulated coupling factor of adiabatic couplers used in the resonator.

To achieve a balance between these two behaviors, we engineer the dispersion of the waveguide using its geometry, resulting in 2.5- μm -wide waveguides with 250 nm of etching depth. The mode profile for a set of representative wavelengths are shown in Fig. 1e, illustrating that the modal overlap remains substantial despite the large frequency difference.

We use adiabatic couplers to create the doubly-resonant cavity. The input and output couplers are identical and, as shown in Fig. 1f, are designed so that signal and idler wavelengths ($\lambda > 1.8 \mu\text{m}$) have large coupling factors ($> 80\%$) while pump wavelengths near $1 \mu\text{m}$ are only slightly coupled ($< 10\%$). The residual coupling of the pump leads to round-trip feedback factors of less than 1% that produce negligible modulations of the pump intensity as a function of frequency, allowing continuous tuning of the pump wavelength.

We fabricate our devices using a commercial wafer (NANOLN) with an x-cut, 700-nm-thick MgO-doped lithium niobate layer and a SiO_2 buffer layer. We provide quasi-phase matching in a 5-mm-long region through periodic poling (inset of Fig. 1b shows a second-harmonic microscope image of a typical poled section). The waveguides are patterned by e-beam lithography and dry etched with Ar^+ plasma. To maximize the spectral range covered on a single chip, we fabricated OPOs with poling periods ranging from $5.55 \mu\text{m}$ to $5.7 \mu\text{m}$ in 10-nm steps. All the OPOs have the same waveguide geometry, with 2.3- μm -wide input and output waveguides that taper (through the adiabatic couplers) to 2.5- μm -wide waveguides inside the resonator. We include a straight waveguide next to each OPO for calibration and quasi-phase matching verification (colored purple in Fig. 1b).

We characterize our OPOs in the quasi-CW regime,

i.e., using pulses that are much longer than the OPO dynamics, so that the OPO reaches steady state during each pulse. This allows us to decrease the average power incident on the chip while maintaining a high peak power. The experimental setup is shown in Fig. 2a, and consists of a tunable CW 1- μm laser amplified by a semiconductor optical amplifier (SOA) that is modulated to generate $\sim 1.45\text{-}\mu\text{s}$ -long (full-width-half-maximum) pulses with 1-kHz repetition rate. The pulses have a triangular shape as a result of the SOA driver bandwidth. These long pulses are further amplified by an ytterbium doped fiber amplifier (YDFA) and coupled into the chip using a single-mode 1- μm lensed fiber (~ 10 dB coupling loss). The OPO output is collected either by a 2- μm lensed fiber, or a cleaved InF_3 fiber, and sent to an optical spectrum analyzer (OSA) or to an InAsSb detector connected to an oscilloscope.

We first characterize a device that operates around degeneracy (Fig. 2b-e). The output wavelengths can be tuned by varying the pump wavelength as shown in Fig. 2b,c. A few spectra are shown in Fig. 2b for different pump wavelengths illustrating operation at signal and idler wavelengths between $1.76 \mu\text{m}$ and $2.51 \mu\text{m}$. We use a mid-infrared OSA for wavelengths above $2.4 \mu\text{m}$ (purple traces). The imbalance between signal and idler levels is due to the different output couplings achieved by the adiabatic couplers at these wavelengths (Fig. 1f). Figure 2c shows several measured (black dots) output wavelengths versus the pump wavelength (the OPO tuning curve) along with the theoretical prediction (black curve and colormap). Operation outside the zero phase mismatch curve ($\Delta k = 0$) is expected since the parametric gain has a finite width around this curve, as shown in the colormap of Fig. 2c. This device can be tuned

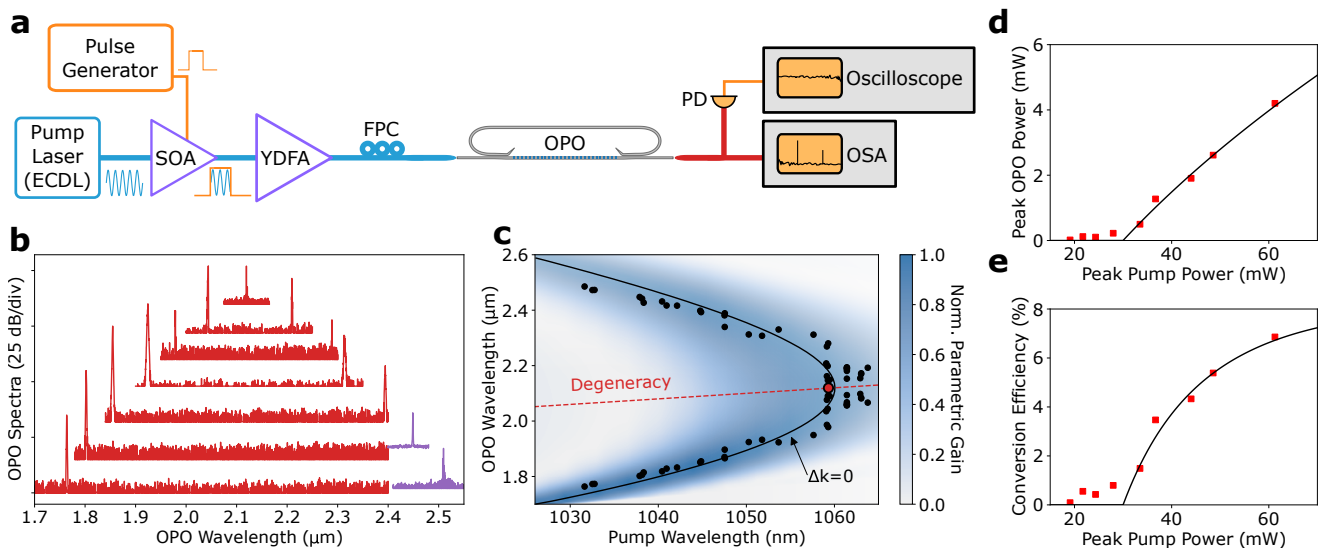


FIG. 2. **Measurements of on-chip doubly-resonant OPOs.** **a**, Quasi-CW measurement setup. We use long triangular pulses ($\sim 1.45\text{-}\mu\text{s}$ full-width-half-maximum with 1-kHz repetition rate) to decrease the average power while keeping the peak power above the OPO threshold. ECDL, external cavity diode laser; SOA, semiconductor optical amplifier; YDFA, ytterbium doped fiber amplifier; FPC, fiber polarization controller; OPO, optical parametric oscillator; PD, photodetector; OSA, optical spectrum analyzer. **b**, OPO output spectra for different pump wavelengths. Each trace shows signal and idler outputs. A mid-infrared OSA was used for wavelengths larger than $2.4\ \mu\text{m}$ (purple traces). **c**, Theoretical tuning curve (solid line) at $25\ ^\circ\text{C}$ (zero phase-mismatch, $\Delta k = 0$) along with measured outputs (dots). The colormap corresponds to the normalized parametric gain with maximum at $\Delta k = 0$. Operation at degeneracy is highlighted in red. **d,e**, Measured OPO on-chip power (signal + idler) and conversion efficiency (e) as a function of on-chip pump power. Solid lines are fits to the theoretical expressions and indicate a threshold of $\sim 30\ \text{mW}$ of on-chip peak power, corresponding to $\sim 42\ \mu\text{W}$ of on-chip average power.

over $750\ \text{nm}$ by varying the pump wavelength by only $30\ \text{nm}$. It can also operate at degeneracy by using a 1060-nm pump as shown in the topmost trace of Fig. 2a, corresponding to the red dot in Fig. 2b.

The measured OPO on-chip output power (signal + idler) is shown in Fig. 2d as a function of on-chip pump power. A theoretical fit reveals an on-chip threshold of $\sim 30\ \text{mW}$ of peak power, corresponding to $\sim 42\ \mu\text{W}$ of on-chip average power. Figure 2e shows the on-chip conversion efficiency, which has an extrapolated maximum value of $\sim 8\%$. This efficiency is limited by the escape efficiency of the OPO (see Supplement 1) which is currently low for the idler, and can be enhanced significantly with different coupler designs.

Figure 3 shows the output spectra of a few more OPOs fabricated on the same chip. These OPOs have longer poling periods for operation far from degeneracy, thus supporting light generation in an extended spectral region that covers an octave. The top panel of Fig. 3 shows just a few spectra, including an OPO that can achieve signal and idler wavelengths separated by more than an octave, and with an idler wavelength well into the mid-infrared. Many more spectra from the same OPOs are shown in the bottom panel, exposing dense coverage over the entire spectral range, except for a band around $\sim 2.8\ \mu\text{m}$ where the SiO_2 buffer layer exhibits an absorption peak [17].

These results show that highly tunable infrared sources can be implemented on chip using the thin-film lithium niobate platform, adding to the increasingly available set of functionalities in this platform [18], and complementing the recent demonstration of a tunable heterogeneously integrated near-infrared laser [19].

Compared to triply-resonant OPOs, a doubly-resonant configuration offers a smoother tuning behavior at the expense of a higher threshold power. While the threshold of our devices is already within the reach of low-cost near-infrared diode lasers, reducing it by a 2-10x factor would make it more attractive. Paths towards this goal include using resonant enhancement of the pump field in a separate cavity (which is more flexible than a triply resonant cavity), increasing the length of the poled section, and improving the quality factor of the resonator. We note here that we are reporting only on-chip power levels, since the input fiber-to-chip coupling loss can be decreased to sub-1-dB levels [20] and doesn't represent a fundamental limitation.

The maximum conversion efficiency of a doubly-resonant OPO is given by its escape efficiency, which is related to the ratio of output coupler transmittance to total resonator losses (see Supplement 1). For our device, this ratio is $\sim 8\%$, indicating that the output coupling is small compared to the total losses in the resonator. This could be caused in part by the little transmission of the

output coupler, particularly at idler wavelengths, and in part by intrinsic resonator losses and losses at the input coupler.

To estimate propagation losses in our waveguides, we have fabricated chips with arrays of critically coupled resonators and extracted quality factors $\sim 6 \times 10^5$, which translate to losses below 0.3 dB/cm. However, this is for waveguides without poling. Detailed inspection of the periodically poled waveguide inside the resonator reveals periodic roughness of the waveguide sidewalls, likely from the polarization dependent etch rate of lithium niobate. More studies are necessary to improve the resonator quality factor.

Input and output couplers play a crucial role in our OPO design. We used adiabatic couplers in this work since they provide a simple means to approximately achieve our requirements of high signal and idler coupling together with low pump coupling. However, significant improvements can be gained by changing the couplers design. The output coupler directly affects the output escape efficiency and an optimum design will have a flat transmission over the desired output wavelength range. The input coupler should, ideally, have 100% coupling at signal and idler frequencies since any transmission in this coupler behaves as additional resonator loss, increasing threshold and reducing efficiency. Simultaneously, the input coupler should provide very low coupling at the pump wavelength, since any coupling just leaks pump power into the unused port, and provides an undesired feedback path for the pump. All these characteristics may be achievable through more advanced coupler designs, for instance, those obtained by inverse design methods [21].

Since the wavelength coverage of the OPO appears to be limited by the loss of the SiO₂ buffer layer, a similar design with a different buffer layer material can allow operation towards the entire lithium niobate transparency window [14]. The OPO design we demonstrate here can also be readily applied to other emerging nonlinear photonic platforms with transparency windows deeper into the mid-infrared [22].

The measurements presented in Fig. 2,3 only exploit the dependence of the output wavelength on pump wavelength. Two additional degrees of freedom are the temperature and the resonator's free spectral range (which could be varied, for instance, by electro-optic modulation of the resonator's feedback arm). These three variables combined can facilitate precise tuning of the output wavelengths over a much broader spectral range [23].

Singly-resonant OPOs offer even smoother tunability and stability characteristics at the expense of higher threshold powers. Such operation can be obtained by changing the coupler response so that only the signal or idler resonates. This could enable fast and ultrabroad wavelength synthesis on-chip with potential mode-hop free operation.

In summary, we have demonstrated on-chip doubly-resonant OPOs that can be tuned over a wide range

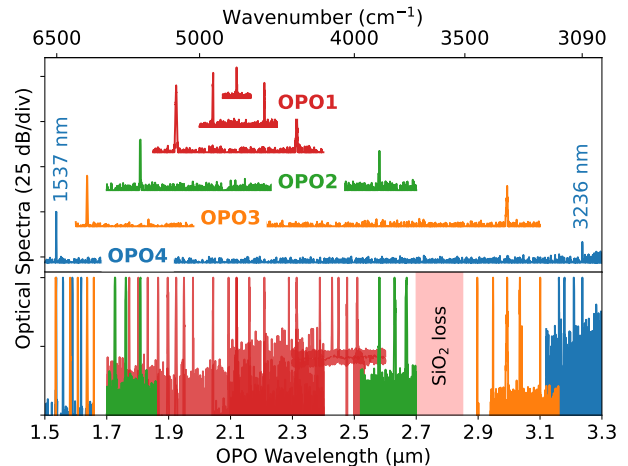


FIG. 3. **Wavelength tuning range.** Top panel shows examples of output spectra for a few OPOs on the same chip exhibiting an octave-wide tuning range. Each color represents a different OPO. Bottom panel shows many more output spectra from the same OPOs.

of wavelengths up to 3.25 μm . This range is already sufficient to cover absorption regions of several importance molecules, including NH₃, CO₂ and several isotopes of CH₄ [3]. Moreover, sum frequency generation between the pump and the OPO signal is observed in our experiments and could be harnessed as a source of tunable visible light within the same chip after subsequent optimizations. Our OPOs are based on a novel on-chip doubly-resonant design that avoids many of the challenges present in triply-resonant configurations and linear cavity oscillators, and can be easily extended to singly-resonant configurations. Also, the ability to perform dispersion engineering makes possible the integration of femtosecond synchronously-pumped OPOs and the numerous applications they unlock [24].

Funding. The authors gratefully acknowledge support from ARO grant no. W911NF-18-1-0285, NSF grant no. 1846273 and 1918549, AFOSR award FA9550-20-1-0040.

Acknowledgment. The device nanofabrication was performed at the Kavli Nanoscience Institute (KNI) at Caltech. This work was supported by a NASA Space Technology Graduate Research Opportunities Award. Part of this research was carried out at the Jet Propulsion Laboratory, California Institute of Technology, under a contract with the National Aeronautics and Space Administration. The authors thank NTT Research for their financial and technical support.

Disclosures. L.L, R.M.B. and A.M: US patent 11,226,538 (P). The remaining authors declare no conflicts of interest.

Data availability. Data underlying the results presented in this papers may be obtained from the authors upon reasonable request.

- [1] A. E. Willner, ed., *Optical Fiber Telecommunications VII* (Academic Press is an imprint of Elsevier, London ; San Diego, CA, 2020).
- [2] Y. Jiang, S. Karpf, and B. Jalali, Time-stretch LiDAR as a spectrally scanned time-of-flight ranging camera, *Nature Photonics* **14**, 14 (2020).
- [3] Gordon et al., The HITRAN2020 molecular spectroscopic database, *Journal of Quantitative Spectroscopy and Radiative Transfer* **277**, 107949 (2022).
- [4] Y. Yao, A. J. Hoffman, and C. F. Gmachl, Mid-infrared quantum cascade lasers, *Nature Photonics* **6**, 432 (2012).
- [5] M. H. Dunn and M. Ebrahimzadeh, Parametric Generation of Tunable Light from Continuous-Wave to Femtosecond Pulses, *Science* **286**, 1513 (1999).
- [6] C. Langrock and M. M. Fejer, Fiber-feedback continuous-wave and synchronously-pumped singly-resonant ring optical parametric oscillators using reverse-proton-exchanged periodically-poled lithium niobate waveguides, *Optics Letters* **32**, 2263 (2007).
- [7] M. Savanier, C. Ozanam, L. Lanco, X. Lafosse, A. Andronico, I. Favero, S. Ducci, and G. Leo, Near-infrared optical parametric oscillator in a III-V semiconductor waveguide, *Applied Physics Letters* **103**, 261105 (2013).
- [8] N. L. B. Sayson, T. Bi, V. Ng, H. Pham, L. S. Trainor, H. G. L. Schwefel, S. Coen, M. Erkintalo, and S. G. Murdoch, Octave-spanning tunable parametric oscillation in crystalline Kerr microresonators, *Nature Photonics* **13**, 701 (2019).
- [9] C. Wang, C. Langrock, A. Marandi, M. Jankowski, M. Zhang, B. Desiatov, M. M. Fejer, and M. Lončar, Ultrahigh-efficiency wavelength conversion in nanophotonic periodically poled lithium niobate waveguides, *Optica* **5**, 1438 (2018).
- [10] L. Razzari, D. Duchesne, M. Ferrera, R. Morandotti, S. Chu, B. E. Little, and D. J. Moss, CMOS-compatible integrated optical hyper-parametric oscillator, *Nature Photonics* **4**, 41 (2010).
- [11] X. Lu, G. Moille, A. Singh, Q. Li, D. A. Westly, A. Rao, S.-P. Yu, T. C. Briles, S. B. Papp, and K. Srinivasan, Milliwatt-threshold visible-telecom optical parametric oscillation using silicon nanophotonics, *Optica* **6**, 1535 (2019).
- [12] X. Lu, G. Moille, A. Rao, D. A. Westly, and K. Srinivasan, On-chip optical parametric oscillation into the visible: Generating red, orange, yellow, and green from a near-infrared pump, *Optica* **7**, 1417 (2020).
- [13] J. Lu, A. A. Sayem, Z. Gong, J. B. Surya, C.-L. Zou, and H. X. Tang, Ultralow-threshold thin-film lithium niobate optical parametric oscillator, *Optica* **8**, 539 (2021).
- [14] J. Mishra, T. P. McKenna, E. Ng, H. S. Stokowski, M. Jankowski, M. Jankowski, C. Langrock, D. Heydari, H. Mabuchi, M. M. Fejer, and A. H. Safavi-Naeini, Mid-infrared nonlinear optics in thin-film lithium niobate on sapphire, *Optica* **8**, 921 (2021).
- [15] A. Marandi, L. Ledezma, Y. Xu, and R. M. Briggs, Thin-film optical parametric oscillators, U.S. Patent 11,226,538.
- [16] L. Ledezma, R. Sekine, Q. Guo, R. Nehra, S. Jahani, and A. Marandi, Intense optical parametric amplification in dispersion-engineered nanophotonic lithium niobate waveguides, *Optica* **9**, 303 (2022).
- [17] H. Lin, Z. Luo, T. Gu, L. C. Kimerling, K. Wada, A. Agarwal, and J. Hu, Mid-infrared integrated photonics on silicon: A perspective, *Nanophotonics* **7**, 393 (2018).
- [18] D. Zhu, L. Shao, M. Yu, R. Cheng, B. Desiatov, C. J. Xin, Y. Hu, J. Holzgrafe, S. Ghosh, A. Shams-Ansari, E. Puma, N. Sinclair, N. Sinclair, C. Reimer, M. Zhang, M. Lončar, and M. Lončar, Integrated photonics on thin-film lithium niobate, *Advances in Optics and Photonics* **13**, 242 (2021).
- [19] C. O. de Beeck, F. M. Mayor, S. Cuyvers, S. Poelman, J. F. Herrmann, O. Atalar, T. P. McKenna, B. Haq, W. Jiang, J. D. Witmer, G. Roelkens, A. H. Safavi-Naeini, R. V. Laer, R. V. Laer, R. V. Laer, and B. Kuyken, III/V-on-lithium niobate amplifiers and lasers, *Optica* **8**, 1288 (2021).
- [20] C. Hu, A. Pan, T. Li, X. Wang, Y. Liu, S. Tao, C. Zeng, C. Zeng, J. Xia, and J. Xia, High-efficient coupler for thin-film lithium niobate waveguide devices, *Optics Express* **29**, 5397 (2021).
- [21] S. Molesky, Z. Lin, A. Y. Piggott, W. Jin, J. Vucković, and A. W. Rodriguez, Inverse design in nanophotonics, *Nature Photonics* **12**, 659 (2018).
- [22] R. Becheker, M. Bailly, S. Idlahcen, T. Godin, B. Gerard, H. Delahaye, G. Granger, S. Février, A. Grisard, E. Lallier, and A. Hideur, Optical parametric generation in OP-GaAs waveguides pumped by a femtosecond fluoride fiber laser, *Optics Letters* **47**, 886 (2022).
- [23] R. C. Eckardt, C. D. Nabors, W. J. Kozlovsky, and R. L. Byer, Optical parametric oscillator frequency tuning and control, *Journal of the Optical Society of America B* **8**, 646 (1991).
- [24] Y. Kobayashi, K. Torizuka, A. Marandi, R. L. Byer, R. A. McCracken, Z. Zhang, and D. T. Reid, Femtosecond optical parametric oscillator frequency combs, *Journal of Optics* **17**, 094010 (2015).